JGP Journal of General Physiology

METHODS AND APPROACHES

Quantitative determination of cellular [Na^+] by fluorescence lifetime imaging with CoroNaGreen

Jan Meyer[1,2], Verena Untiet[2], Christoph Fahlke[2], Thomas Gensch[2], and Christine R. Rose[1]

Fluorescence lifetime imaging microscopy (FLIM) with fluorescent ion sensors enables the measurement of ion concentrations based on the detection of photon emission events after brief excitation with a pulsed laser source. In contrast to intensity-based imaging, it is independent of dye concentration, photobleaching, or focus drift and has thus been successfully employed for quantitative analysis of, e.g., calcium levels in different cell types and cellular microdomains. Here, we tested the suitability of CoroNaGreen for FLIM-based determination of sodium concentration ([Na^+]) inside cells. In vitro measurements confirmed that fluorescence lifetimes of CoroNaGreen (CoroNaFL) increased with increasing [Na^+]. Moreover, CoroNaFL was largely independent of changes in potassium concentration or viscosity. Changes in pH slightly affected FL in the acidic range (pH ≤ 5.5). For intracellular determination of [Na^+], HEK293T cells were loaded with the membrane-permeable form of CoroNaGreen. Fluorescence decay curves of CoroNaGreen, derived from time-correlated single-photon counting, were approximated by a bi-exponential decay. In situ calibrations revealed a sigmoidal dependence of CoroNaFL on [Na^+] between 0 and 150 mM, exhibiting an apparent K_d of ∼80 mM. Based on these calibrations, a [Na^+] of 17.6 mM was determined in the cytosol. Cellular nuclei showed a significantly lower [Na^+] of 13.0 mM, whereas [Na^+] in perinuclear regions was significantly higher (26.5 mM). Metabolic inhibition or blocking the Na^+/K^+-ATPase by removal of extracellular K^+ caused significant [Na^+] increases in all cellular subcompartments. Using an alternative approach for data analysis ("Ratio FLIM") increased the temporal resolution and revealed a sequential response to K^+ removal, with cytosolic [Na^+] increasing first, followed by the nucleus and finally the perinuclear regions. Taken together, our results show that CoroNaGreen is suitable for dynamic, FLIM-based determination of intracellular [Na^+]. This approach thus represents a valuable tool for quantitative determination of [Na^+] and changes thereof in different subcellular compartments.

Introduction

A fundamental property of animal cells is that they maintain a low sodium concentration ([Na^+]) in their cytosol. This is accomplished by the ubiquitous Na^+/K^+-ATPase (NKA), which converts ATP into energy stored in an inwardly directed Na^+ gradient across the plasma membrane (Sweadner, 1989; Kaplan, 2002). The Na^+ gradient is used to drive secondary-active transporters including ion transporters such as the Na^+/Ca^{2+} exchangers (Verkhratsky et al., 2018) or transporters for metabolites (Wright and Turk, 2004). Increases in the cytosolic [Na^+], e.g., following channel-mediated Na^+ influx (Rose et al., 1999), may result in a reduction or even reversal of Na^+-dependent transporters, a phenomenon described for Na^+/Ca^{2+} exchange in the heart muscle or in the brain (Kirischuk et al., 2012; Aronsen et al., 2013; Gerkau et al., 2018). Na^+-dependent transporters are expressed not only at the plasma membrane but also at the membranes of cellular organelles. Mitochondria, for example, express Na^+/Ca^{2+} exchangers that shape mitochondrial calcium signaling in a Na^+-dependent manner, thereby regulating mitochondrial as well as cellular functions (Maack et al., 2006; Murphy and Eisner, 2009; Parnis et al., 2013; Nita et al., 2014; Ben-Kasus Nissim et al., 2017).

The foresaid studies thus indicate that there is a tight interrelationship between regulation and signaling of Na^+ and other ions, which not only includes the cytosol but also comprises intracellular organelles. Detailed understanding of these processes requires knowledge on driving forces, which means knowledge on basal [Na^+] as well as changes thereof during signaling in the various subcellular compartments. Determination of [Na^+] has, however, always been hampered by the limited availability of experimental tools. In essence, only a handful of chemical fluorescent indicators suitable for dynamic Na^+ imaging inside cells exist and all suffer from well-known pitfalls such as interaction with proteins and

[1]Institute of Neurobiology, Faculty of Mathematics and Natural Sciences, Heinrich Heine University Düsseldorf, Düsseldorf, Germany; [2]Institute of Complex Systems 4 (ICS-4), Zelluläre Biophysik, Forschungszentrum Jülich, Jülich, Germany.

Correspondence to Christine R. Rose: rose@hhu.de; V. Untiet's present address is Center for Translational Neuromedicine, Faculty of Health and Medical Sciences, University of Copenhagen, Copenhagen, Denmark.

other cellular constituents or low quantum efficacy and bleaching (Schreiner and Rose, 2012; Biskup and Gensch, 2014). The latter is especially critical when measurement of [Na^+] is based on the analysis of the emission intensity of the dyes.

In addition to exhibiting a change in fluorescence intensity with ion binding, many ion-selective fluorescent dyes also show a change in their fluorescence lifetime (FL), a parameter that is independent from the number of dye molecules (Bastiaens and Squire, 1999). In FL imaging microscopy (FLIM; Suhling et al., 2005; Becker, 2012), a pulsed laser source can be employed in combination with time-correlated single-photon counting (TCSPC). The latter records the exact time at which individual photons hit the detector after the excitation event. The temporal incidence of photon emission decays exponentially, and repeating this measurement many times enables the construction of a curve from which the average FL is deducted. As mentioned above, the FL is generically independent from the absolute number of dye molecules and from dye concentration.

Since its first implementation for intensity-independent, quantitative analysis of calcium concentrations in 1992 (Lakowicz et al., 1992), this technique has been widely employed for determination of intracellular calcium in different tissues (Wilms et al., 2006; Wilms and Eilers, 2007). Among others, Ca^{2+}-FLIM revealed globally increased calcium concentrations in astrocytes close to amyloid plaques in mouse models of Alzheimer's disease (Kuchibhotla et al., 2009) or demonstrated different resting calcium levels along dendrites of hippocampal neurons in rat brain tissue (Zheng et al., 2015). FLIM of ion indicators has also been employed for determination of intracellular chloride concentrations, e.g., in olfactory epithelia (Kaneko et al., 2004), dorsal root ganglia of rodents (Gilbert et al., 2007), cockroach salivary acinar cells (Lahn et al., 2011), cells of the mouse vomeronasal organ (Untiet et al., 2016), or acute slices of mouse brain (Untiet et al., 2017).

Up to now, FLIM-based analysis of [Na^+] has only been performed in a couple of studies, and some of these focused on cell-free systems only (Szmacinski and Lakowicz, 1997; Despa et al., 2000b; Roder and Hille, 2014; Naumann et al., 2018). Recently, the chemical sodium indicator dye CoroNaGreen was employed for FLIM-based detection of somatic [Na^+] increases in neurons in mouse brain tissue (Rungta et al., 2015), but no further characterization and evaluation of the dye's properties, such as its sensitivity to potassium or pH, or a calibration to reveal its apparent K_d in situ, were performed. The goal of the present work was therefore to analyze the suitability of lifetime measurements of CoroNaGreen for quantitative determination of intracellular [Na^+] in more depth. In addition, we tested if CoroNaGreen FLIM can be employed to monitor changes in [Na^+] induced by metabolic inhibition or inhibition of the cellular NKA. To this end, we employed two different strategies for data analysis: TCSPC as well as a photon-count ratio method ("Ratio FLIM"), with the latter increasing the temporal resolution several-fold as compared with the former.

Materials and methods

FL determination of CoroNaGreen in vitro

To determine the properties of CoroNaGreen (Life Technologies, Thermo Fisher Scientific; C36675) in vitro, the dye was dissolved at 5 µM in 1 ml saline composed of 10 mM HEPES, 26 mM K^+-gluconate, and different [Na^+] (0–150 mM); [K^+] was adjusted to maintain iso-osmolarity (NaCl + KCl = 150 mM), and pH was titrated to 7.3 with KOH. To evaluate the K^+-sensitivity of CoroNaGreen, [Na^+] was set to 15 mM and [K^+] was varied between 30 and 150 mM, while NMDG was added accordingly to maintain iso-osmolarity. To analyze its dependence on pH, salines with 20 mM [Na^+] were used in which pH was adjusted between 5.0 and 8.0. The influence of different viscosity was tested using a saline with 20 mM Na^+, to which 0, 1, 3, or 5% (g/ml) of an 80 kD dextran (Sigma-Aldrich Chemie; 00892) was added.

The time-resolved detection of CoroNaGreen's fluorescence decay in vitro was performed with a Fluotime100 fluorescence spectrophotometer based on a picoHarp300 unit (PicoQuant). As an excitation source, a pulsed diode laser (LDH-440; center wavelength, 440 nm; pulse width, 54 ps; repetition frequency, 20 MHz; PicoQuant) was used. Fluorescence decay curves were measured by a photomultiplier, where photons were spectrally selected by a monochromator (530 nm, CoroNaGreen; or 440 nm, Instrument Response Function [IRF]) and acquired in TCSPC mode. Fig. 1, A, C, E, and G, depict the nonconvolved, as-measured fluorescence decay curves. For further processing, the fluorescence decay curves were analyzed by iterative reconvolution of a bi-exponential model function and the measured IRF using the software package FluoFit 4.4 (PicoQuant). Fig. 1, B, D, F, and H, show the average FL calculated from the respective bi-exponential model function (see also below).

Cell culture and dye loading

HEK293T cells ("HEK cells"; human embryonic kidney, 96121229, SV40 transformed) were obtained from the European Collection of Cell Cultures (Sigma-Aldrich Chemie). Cells were grown using Dulbecco's modified Eagle's medium, 10% FBS, supplied with 1% penicillin streptomycin (10,000 units/ml penicillin stock, 10,000 µg/ml streptomycin stock, GIBCO, Thermo Fisher Scientific) and 2 mM glutamine (Thermo Fisher Scientific). The cells were trypsinized and replated twice a week when they reached 70–80% confluence.

For experiments, coverslips were transferred to an experimental bath and incubated in artificial cerebrospinal fluid (ACSF), composed of 125 mM NaCl, 3 mM KCl, 25 mM HEPES, 2 mM $MgSO_4$, 2 mM $CaCl_2$, 1.25 mM NaH_2PO_4, and 5 mM glucose, titrated to pH 7. For dye-loading, cells were incubated with the membrane-permeable form of CoroNaGreen (CoroNaGreen acetoxymethyl [AM] ester; C36676; Thermo Fisher Scientific) dissolved (15 µM) in ACSF for 15 min at room temperature. After dyeloading, HEK cells were washed with ACSF and placed in an imaging chamber of an upright scanning fluorescence microscope (A1R MP; Nikon Instruments Europe). In some experiments, cells were additionally stained with 15 nM MitoTracker Red CMXRos ("Mitotracker") for 15 min at 36°C (M7512; Thermo Fisher Scientific) before loading the cells with CoroNaGreen-AM at room temperature as described above.

FL imaging and calibration of CoroNaGreen in situ

Dye-loaded HEK cells were excited by 100 fs pulses at 880 nm, generated at 80 MHz by a mode-locked Titan Sapphire laser

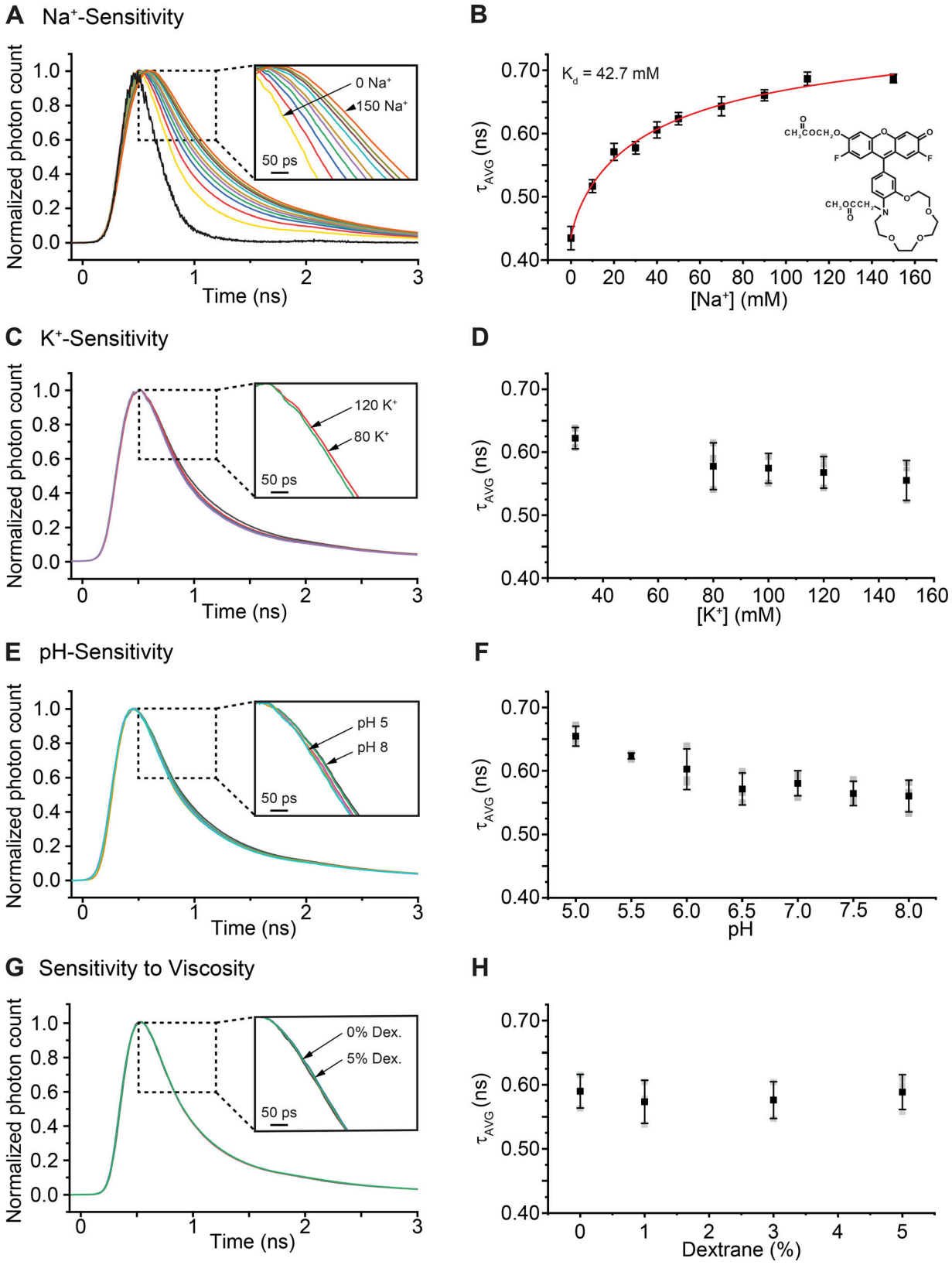

Figure 1. **Ion dependence of CoroNaGreen FL in vitro.** Traces shown on the left (A, C, E, and G) represent temporal photon distributions emitted by CoroNaGreen (normalized photon count) after pulsed excitation in different salines as indicated; the insets show an enlargement of the fluorescence intensity decays as a function of time between 0.5–1.2 ns. Graphs on the right (B, D, F, and H) illustrate mean values of τ_{AVG} ± SD obtained from three experiments each. **(A and B)** Photon count and τ_{AVG} of CoroNaGreen in salines with different [Na^+], ranging from 0–150 mM. Data in B were fit with a sigmoidal function, revealing a K_d of 42.7 mM. In A, the IRF is shown in black. **(B)** Also depicted is the structural formula of CoroNaGreen as given by the

manufacturer. **(C and D)** Photon count and τ_{AVG} of CoroNaGreen in salines with a fixed [Na^+] of 15 mM and potassium concentrations altered between 30 and 150 mM (plotted are 30, 80, 100, 120, and 150 mM). The inset on the left illustrates the nearly complete overlap obtained at 80 and 120 mM [K^+]. **(E and F)** pH sensitivity of photon count and τ_{AVG} of CoroNaGreen at a given [Na^+] of 20 mM. Plotted are traces obtained at pH 5.0, 5.5, 6.0, 6.5, 7.0, 7.5, and 8.0. **(G and H)** Photon count and τ_{AVG} of CoroNaGreen at a [Na^+] of 20 mM and after addition of dextran at 1, 3, and 5%. Note that addition of dextran did not result in a detectable change in fluorescence intensity decays.

(Mai Tai DeepSee, Newport, Spectra Physics; excitation power 3–15 mW (typically 5 mW). Fluorescence emission intensity of CoroNaGreen was detected using a 534/30 band-pass filter (F39-533; AHF Analysentechnik AG) using an upright fluorescence microscope (A1 MP; Nikon) equipped with a 25× water immersion objective (numerical aperture 1.1; working distance 2 mm; CFI75 Apochromat 25XC W; Nikon). Mitotracker fluorescence intensity was collected using a 575-nm long-pass filter; a 540 nm short-pass filter was used for FL imaging of CoroNaGreen (575 LP [SKU: XF3089/25] and 540 SP [SKU: RPE540SP], both from Omega Optical).

Average FLs were determined using multidimensional TCSPC in a volume of 0.08 µm³ per individual pixel. Fluorescence emission was detected with a GaAsP hybrid photodetector (HPM-100-40; Becker & Hickl). TCSPC electronics (SPC-150; Becker & Hickl) and acquisition software (SPCM, Becker & Hickl) were used for obtaining FL images as previously described (Untiet et al., 2017). If not stated otherwise, pixel dwell time was 15.26 µs for frames consisting of 512 × 512 pixels; for a total photon count of >3,500 photons per pixel, 20 frames were collected for 80 s, generating one final image.

Generated images were analyzed using a binning of 1 with 3 × 3 pixels and decay curves were analyzed by iterative reconvolution of the instrument response function, $IRF_{(t)}$, with a bi-exponential model function, $M_{(t)}$, using the SPCImage Software (version 6.1; Becker & Hickl) and the following equations (Becker, 2005):

$$I\,(t) = IRF\,(t)\ \times\ M\,(t) \tag{1}$$

and

$$M\,(t) = \sum_{i=1-2}\left[\alpha_i\ \times \exp\left(-\frac{t}{\tau}\right)\right], \tag{2}$$

where τ_i are the characteristic lifetimes and α_i are the respective intensities. The average lifetime, τ_{AVG}, was calculated as (Becker, 2005):

$$\tau_{AVG}\ =\ \frac{\sum_{i=1-2}[\alpha_i\ \times\ \tau_i]}{\sum_{i=1-2}[\alpha_i]}. \tag{3}$$

Subsequently, ImageJ (Schneider et al., 2012) was used to define selected cellular regions of interest (ROI) and τ_{AVG} for each ROI analyzed.

To determine the [Na^+] sensitivity of the FL decay of CoroNaGreen in situ, HEK cells were incubated in ACSF and dye loaded as described above. After obtaining at least two complete images (each at 20 frames) under baseline conditions, cells were exposed to salines containing (in mM): 10 HEPES, 26 K^+-gluconate, 0–150 [Na^+], 0–150 [K^+] (NaCl + KCl = 150 mM); pH titrated to 7.3 with KOH. Cell plasma membranes were permeabilized for Na^+ by additionally using 3 µM gramicidin (Na^+-ionophore; Sigma-Aldrich Chemie), 10 µM monensin (Na^+/H^+-exchanger; Sigma-Aldrich Chemie), and 1 mM ouabain (NKA inhibitor; Calbiochem, Merck KGaA; Rose and Ransom, 1996a; Meier et al., 2006).

τ_{AVG} values obtained were plotted as a function of [Na^+] and fitted with OriginPro Software (OriginLab). A sigmoidal fit function,

$$y\ =\ \frac{\tau_{AVG2}\ +\ (\tau_{AVG1}\ -\ \tau_{AVG2})}{(1+\ \left(\frac{[Na^+]}{K_d}\right)^P)}, \tag{4}$$

was used with τ_{AVG2} = 1,286.3 ps, τ_{AVG1} = 482.6 ps, K_d = 79.9 ± 24.5 mM, and P = 1.26 (R^2 = 0.99), to describe the correlation between FL and different sodium concentrations ([Na^+]).

"Ratio FLIM"

To increase the temporal resolution of TCSPC-based FLIM, we split the fluorescence intensity decay curve into an early (1: 1.12–1.37 ns) and a late segment (2: 1.37–11.52 ns) as introduced earlier (Minge et al., 2017; Zheng et al., 2018). The data derived from the TCSPC-based in situ calibration of CoroNaGreen were then reanalyzed using this procedure. The calculated ratio of the slow to fast photon numbers ("R") was plotted against the sodium concentration and fitted by a sigmoidal function {[(R1 − R2) / (1 + ([Na^+] / K_d)^P] + R2)}, with R1 = 2.95, R2 = 5.64, $[Na^+]_{1/2}$ = 88.6, and P = 1.45 (R^2 = 0.97). Dynamic measurements were performed with 4 s per image (512 × 512) of photon counting, with an additional 4 s required for saving the image file. The resulting total temporal resolution was 8 s.

Analysis and statistics

Unless stated otherwise, all data represent mean values ± SD, calculated using Excel Software (Microsoft). Statistical analysis of the data was performed with OriginPro Software (OriginLab) using a one-way ANOVA to test for normal distribution followed by Tukey's test. Asterisks indicate the level of significance (***, P < 0.001; **, P < 0.01; and *, P < 0.05). If not stated otherwise, *n* represents the number of cells. Each set of experiments on HEK cells was performed on at least three different coverslips.

Results

Properties of CoroNaGreen FL in vitro

CoroNaGreen is a fluorescent dye suitable for dynamic, intensity-based imaging of changes in intracellular sodium concentration ($[Na^+]_i$) of brain cells (Meier et al., 2006). Recent work has also shown that CoroNaGreen exhibits changes in FL with changes in the sodium concentration ([Na^+]) in vitro (Naumann et al., 2018). We first aimed to replicate this observation by performing time-resolved detection of the

fluorescence decay of CoroNaGreen in cuvette calibrations (n = 3 experiments). As reported before (Naumann et al., 2018), the FL of CoroNaGreen increased with increasing [Na^+] (Fig. 1 A). Fitting the data obtained using a sigmoidal plot revealed a K_d of 42.7 ± 18.2 mM (Fig. 1 B). Because baseline [Na^+] inside cells is typically in the range of 10–20 mM, this indicates that CoroNaGreen might be suitable for FLIM-based analysis of [Na^+] inside cells.

We next went on to test its sensitivity to other ions and to changes in viscosity. Vertebrate cells typically maintain a baseline intracellular [K^+] concentration ($[K^+]_i$) of 110–130 mM (Ballanyi et al., 1983; Kofuji and Newman, 2004), which, e.g., in neurons may be transiently reduced due to K^+ loss in response to opening of K^+-permeable ion channels. To test the sensitivity of CoroNaGreen to K^+, we exemplarily compared its FL in salines with a fixed [Na^+] of 15 mM, to reflect baseline conditions, and different [K^+], ranging from 30 to 150 mM (n = 3 experiments). Fig. 1, C and D, illustrate that CoroNaGreen exhibited only small changes in its FL upon varying [K^+]; decay curves were essentially indistinguishable between 120 and 80 mM K^+. Given that [K^+] decreases inside cells are expected to largely mirror concomitant increases in [Na^+] and anticipated changes in [Na^+] are <50 mM, the K^+-sensitivity of CoroNaGreen thus seems negligible for measurements under our experimental conditions in situ.

To probe for the pH sensitivity of CoroNaGreen FL, salines with a fixed [Na^+] of 20 mM and different pH, ranging from 5 to 8, were prepared (n = 3 experiments). As illustrated in Fig. 1, E and F, the FL of CoroNaGreen was essentially independent on pH in the range between 6.0 and 8.0, whereas at pH ≤5.5, FL increased slightly. Finally, we evaluated the effect of different viscosity by adding 80 kD dextran at 0, 1, 3, or 5% to saline with a [Na^+] of 20 mM (n = 3 experiments), where no apparent influence of dextran concentration, i.e., viscosity, on CoroNaGreen FL was detected (Fig. 1, F and G).

Taken together, these data confirm that CoroNaGreen FL changes with changes in [Na^+] in the range between 0 and 150 mM. Moreover, they show that CoroNaGreen FL does not exhibit a significant sensitivity to changes in [K^+] between 80 and 120 mM or in pH in the range between pH 6 and 8. Moreover, no obvious influence of differences in viscosity on CoroNaGreen FL was detected.

In situ calibration of CoroNaGreen FL and determination of baseline [Na^+]

To evaluate the suitability of CoroNaGreen for FL-based imaging of [Na^+] sodium inside cells, we performed a full calibration of CoroNaGreen FL in situ, using HEK cells. To this end, cells were loaded with the membrane-permeable ester form of the dye (CoroNaGreen-AM). Notably, in-homogeneities of FL and emission intensity were detected in different subcellular compartments of dye-loaded cells in standard ACSF (Fig. 2, A and B; see also Fig. 3, A and D). The most obvious and consistent difference concerned a circular region of increased FL/intensity located around the nucleus ranging partly into the cytosol. In addition, dots of higher FL/intensity were also found in cytosolic areas (Fig. 2, A and B; see also Fig. 3, A and D).

To address the identity of the high FL/intensity compartments, cells were additionally stained with Mitotracker, which selectively labels mitochondria (Fig. 2 C). Merging the different channels revealed that compartments exhibiting a distinctly increased FL and intensity showed a remarkable spatial overlap with the Mitotracker fluorescence (Fig. 2, D and E), indicating that they contain a high number and density of mitochondria. This colocalization was especially obvious in the peri-nuclear region (see white areas in the merged images in Fig. 2). Notably, this does not exclude the copresence of other organelles like lysosomes in the region of the high coincident presence of both fluorescent signals.

To calibrate FL of CoroNaGreen in situ, cells were first exposed to ACSF followed by different calibration salines, containing a defined [Na^+] ranging from 0 to 150 mM, as well as ouabain (1 mM), gramicidin (3 µM), and monensin (10 µM; Fig. 3 A; $n \geq 25$). Importantly, the latter ionophores preferentially insert into the plasma membrane and not into organelles (Harootunian et al., 1989), allowing rapid equilibration between the [Na^+] of the cytosol with that of the external saline (Rose and Ransom, 1996a; Langer and Rose, 2009). Under these conditions, the difference in FL between the perinuclear region and the remainder of the cell was largely maintained, and FL was consistently longer for [Na^+] ≤50 mM (Fig. 3 A). At higher [Na^+], however, compartments could no longer be clearly distinguished based on their FL (Fig. 3 A).

To analyze the behavior of the different cellular regions separately, ROIs were manually drawn based on differences in the intensity of CoroNaGreen to delineate the nucleus, perinuclear regions, and cytosol, respectively (see Fig. 3 D). Plotting the FL of the different compartments against the [Na^+] confirmed their apparent divergence at low [Na^+]: while mean FL of nuclei and cytosol were not significantly different for [Na^+] ≤50 mM, FL of perinuclear regions was consistently higher than that of both nuclei and cytosol. This consistent difference was lost for mean values of the FL of the three compartments at [Na^+] ≥70 mM (Fig. 3 B). These results suggested that at [Na^+] relevant for the present study (0–50 mM), [Na^+] was apparently fully equilibrated between cytosol and nucleus. In contrast to this, full equilibration was apparently not obtained for the perinuclear region. Therefore, these ROIs were excluded for the determination of the [Na^+] sensitivity of CoroNaGreen FL in situ. Instead, only ROIs positioned over cytosolic and nuclear regions were included to construct a calibration curve. Plotting the average FL from these ROIs against the [Na^+] revealed an increase from ∼483 ps at 0 mM Na^+ to ∼1,032 ps at 150 mM ($n \geq 25$; Fig. 3 C). Changes in FL followed a sigmoidal function, revealing an apparent K_d of 79.9 ± 24.5 mM (Fig. 3 C).

Using these calibration parameters to the entire cell (ROIs positioned to include all cellular compartments) resulted in an average intracellular [Na^+] ($[Na^+]_i$) of 19.0 ± 4.0 mM in ACSF (n = 58). Based on the observation that FL and intensity differ between cellular regions (see Fig. 2 B), we then determined the FL from three distinct cellular ROIs of each cell separately, comprising (1) the nucleus, (2) the perinuclear region, and (3) the remaining cytosol. This analysis revealed an average [Na^+] in the cytosol ($[Na^+]_c$) of 17.6 ± 4.5. The nuclear [Na^+] ($[Na^+]_n$) was

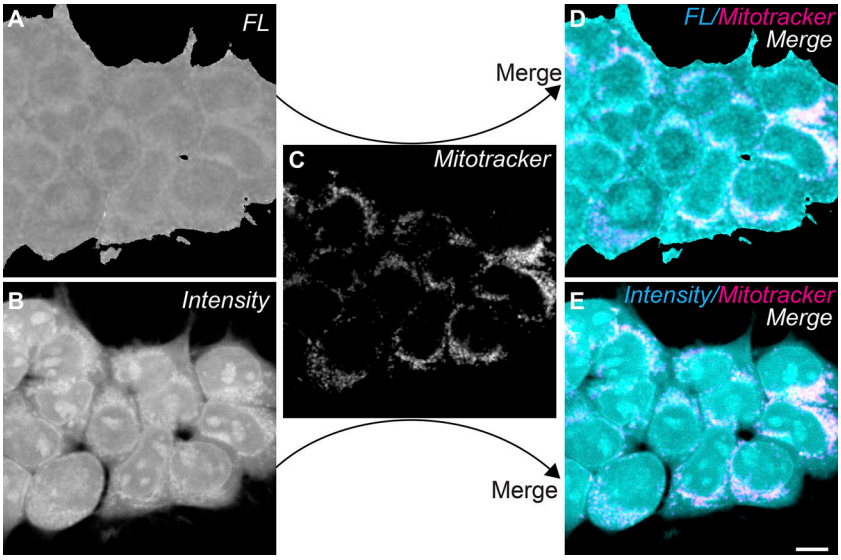

Figure 2. **Identification of cellular subcompartments. (A and B)** HEK cells were loaded with CoroNaGreen-AM in ACSF. **(A)** FL image; dark pixels represent short FL, bright pixels long FL. **(B)** Corresponding image showing the emission intensity of CoroNaGreen. **(C)** Same field of view, showing the cells labeled with Mitotracker. **(D and E)** Merge (white) of Mitotracker fluorescence (magenta) with CoroNaGreen FL (cyan, D) or CoroNaGreen intensity (cyan, E). Scale bar, 20 µm.

significantly lower, amounting to 13.0 ± 4.2 mM. Perinuclear regions, in contrast, exhibited a significantly higher $[Na^+]$ ($[Na^+]_{pn}$) of 26.5 ± 4.8 mM (n = 58; Fig. 3 D).

$[Na^+]$ changes revealed by CoroNaGreen FLIM

The experiments described above show that FL of CoroNaGreen allows quantitative determination of baseline intracellular $[Na^+]$. In a next step, we tested if this technique also enables detection of changes in $[Na^+]$ in the different subcellular compartments upon different experimental manipulations.

First, we analyzed the effect of an inhibition of cellular energy metabolism by perfusing cells with glucose-free saline containing sodium azide (NaN_3; 5 mM), a blocker of mitochondrial ATP production, and 2-desoxyglucose (1 mM), a blocker of glycolysis, for a period of 2 min (n = 20). This is expected to result in a decrease in cellular ATP and thereby in an inhibition of the NKA (Gerkau et al., 2018; Lerchundi et al., 2018). Because the generation of one image required collection of photons for a period of 80 s, one image under baseline conditions (ASCF) was taken first ("T80"), before exposing the cells to the metabolic inhibitors and generating three more images ("T160, T240, T320"; Fig. 4 A). At T320, $[Na^+]$ in all three compartments had increased significantly as compared with baseline conditions (T80): in the cytosol, $[Na^+]$ rose by 7.4 ± 1.8 mM, in the nucleus by 6.7 ± 2.2 mM, and in the perinuclear region by 6.2 ± 2.4 mM (Fig. 4 A). While these three compartments exhibited different baseline $[Na^+]$ (Fig. 4 A) as described before (see Fig. 3 D), the relative changes in $[Na^+]$ induced by metabolic inhibition as well as the general time course detected by this method were similar.

In addition, we analyzed the effect of a perfusion with nominally K^+-free saline for 1 min, which causes an immediate inhibition of the NKA (e.g., Rose and Ransom, 1996a; Kelly and Rose, 2010). Analysis of the FL revealed a significant increase in $[Na^+]$ of all subcompartments in response to switching to K^+-free saline (n = 24; Fig. 4 B). At T320, $[Na^+]$ had increased by 15.8 ± 5.7 mM in the cytosol, by 15.8 ± 3.8 mM in the nucleus, and by 12.9 ± 4.7 mM in the perinuclear region. While the relative changes compared with baseline $[Na^+]$ were highly significant for each compartment, the overall responses of the different compartments were again similar. As observed with metabolic inhibition (see Fig. 4 A), $[Na^+]$ did not recover to baseline (Fig. 4 B), suggesting that NKA was still not fully operational within the given observation window.

Taken together, these experiments show that FLIM of CoroNaGreen can be employed to determine absolute changes in $[Na^+]$ in cellular compartments in response to different manipulations. Inherent to the long acquisition times, necessary to construct reliable fits of fluorescence decay times, however, the temporal resolution is rather low.

$[Na^+]$ changes revealed by "Ratio FLIM"

Conventional, time-domain TCSPC-based FLIM relies on the determination of τ_{AVG} by fitting a bi-exponential decay function to the fluorescence intensity time course. As stressed above, relatively large photon numbers (2,000 or more under our experimental conditions; Rahmati, S., T. Gensch, and F.Z. Jülich, personal communication) are needed in every pixel to obtain a reliable fit of the bi-exponential function to the pixel's fluorescence intensity decay as a function of time causing relatively long acquisition times of ∼80 s.

To increase the temporal resolution of TCSPC-based FLIM, an alternative approach based on splitting the fluorescence intensity decay curve into early and late segments and estimating the number of photons in the two time periods was introduced earlier (Zheng et al., 2015, 2018; Minge et al., 2017). If the fluorescence decay of the measured compound (here CoroNaGreen) will change due to Na^+ binding to the dye, the relative amount of photons in the early and late time period will change. The optimal value for splitting the decay curve cannot be calculated in general but needs to be determined for a given setup and fluorescent molecule.

We tested different splitting values and determined segment 1 from 1.12 to 1.37 ns and segment 2 from 1.37 to 11.52 ns as the best suited for our measurements. By calculating the ratio of the photon numbers of the two segments (Fig. 5 A), one obtains a parameter that reflects changes in the fluorescence decay profile

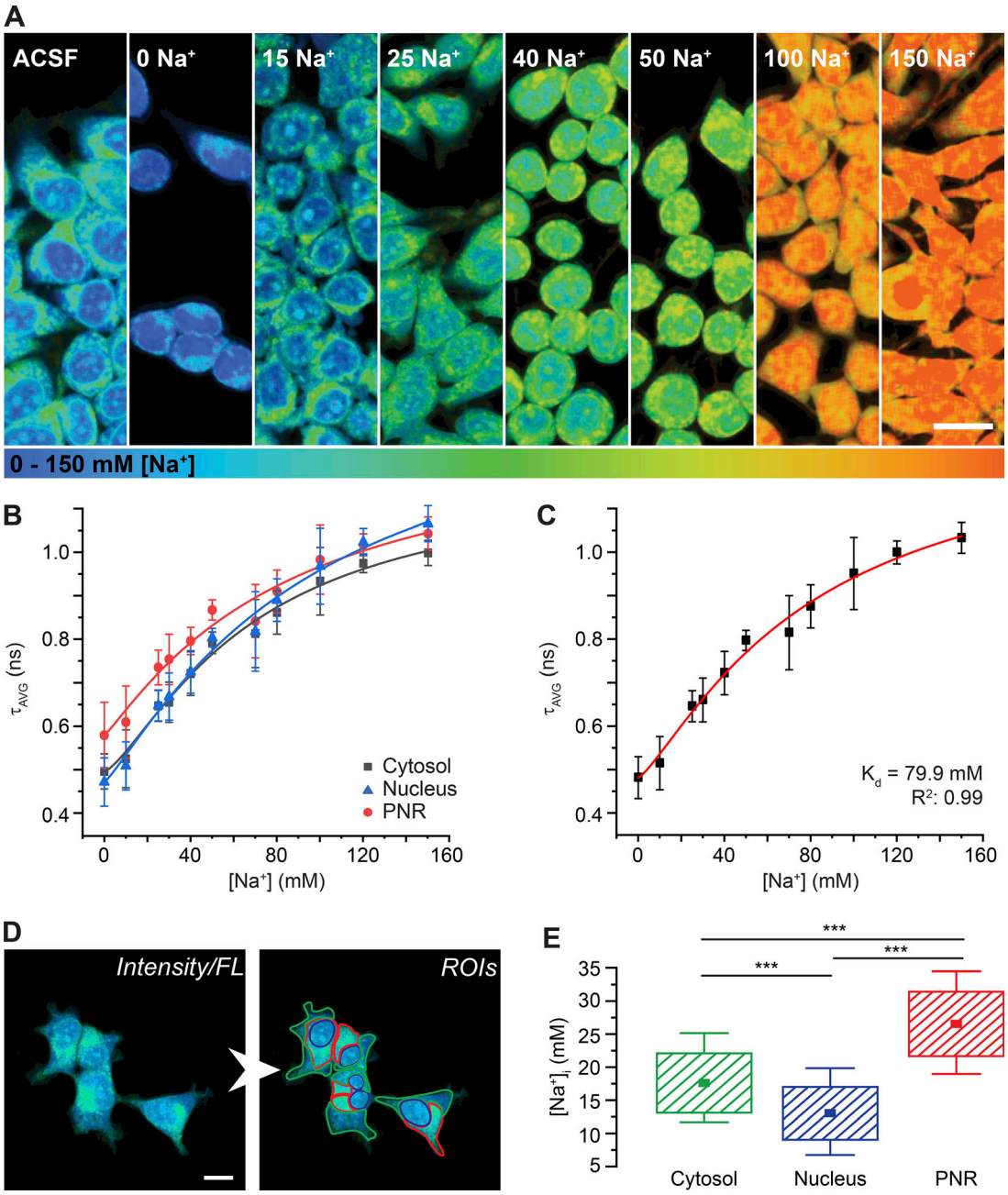

Figure 3. **In situ calibration of CoroNaGreen. (A)** Color-coded FL images of HEK cells loaded with CoroNaGreen-AM. Blue colors represent low [Na^+], and red colors represent high [Na^+] as indicated by the color-coding bar below the image. First image (left) was obtained in ACSF, after which cells were exposed to calibration solutions containing [Na^+] ranging from 0–150 mM as indicated. **(B)** Mean values of τ_{AVG} ± SD in ROIs, representing the cytosol, nucleus, and perinuclear region (PNR). Data are fit using a sigmoidal function. Note that values for PNR are consistently well above those for cytosol and nucleus for [Na^+] ≤50 mM. **(C)** Mean values of τ_{AVG} ± SD in ROIs obtained from cytosol and nucleus and a sigmoidal fit of the data revealing a K_d of 79.9 mM. **(D)** Left: FL image of HEK cells, color-coded as in A. Right: Same image with regions of interest for cytosol (green), nucleus (blue) and perinuclear regions (red) indicated. **(E)** Box plot showing mean [Na^+] (square), SD (box), and 5/95 percentiles (whiskers) in the cytosol, nucleus, and PNRs of HEK cells. **(A and D)** Scale bars, 20 µm. **(E)** ***, P ≤ 0.001.

similar to those reported by τ_{AVG}. The calculated ratio of the slow to fast photon numbers ("R") is dependent on the change of the fluorophores' fluorescence decay property, which in the case of CoroNaGreen is a measure of Na^+ binding and hence [Na^+]. Then the data derived from in situ calibrations of CoroNaGreen (0–150 mM Na^+, 14 conditions, $n \geq 25$; see Fig. 3 B) were reanalyzed. When plotting the resulting ratio versus the [Na^+] (Fig. 5 B), data could be fitted by a sigmoidal function. The apparent K_d of 88.6 mM was close to that determined based on fitting decay curves (79.9; see Fig. 3 B).

Subsequently, we employed Ratio FLIM in a new set of experiments to study the response of HEK cells to removal of extracellular K^+ for 1 min (n = 21). Analysis was performed on images generated within 8 s (collecting photons for 4 s followed

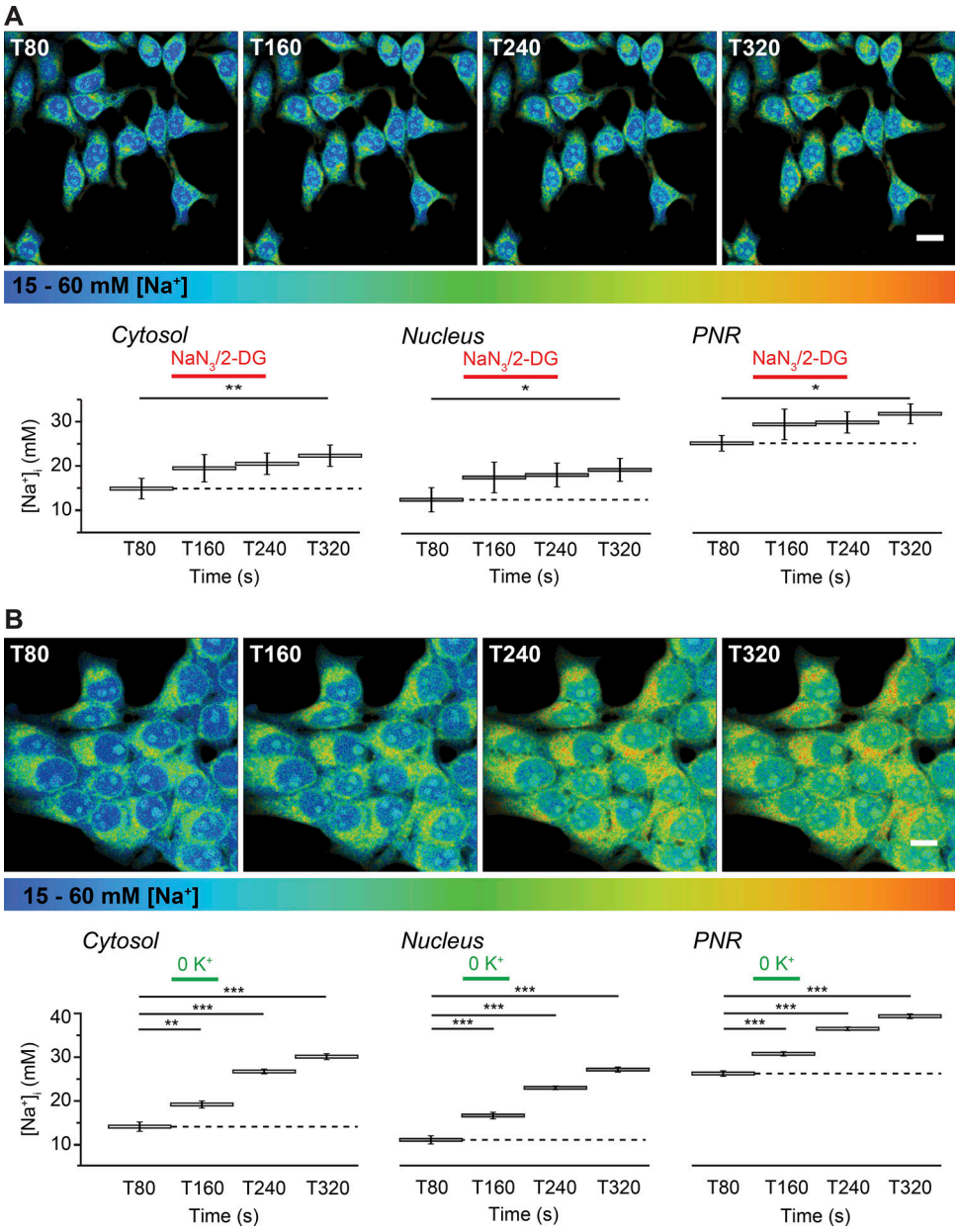

Figure 4. **[Na⁺] changes detected by FLIM of CoroNaGreen: (A)** Top: FL images of CoroNaGreen-AM-loaded HEK cells under control conditions (ACSF) and in response to perfusion with glucose-free saline containing sodium azide (NaN_3; 5 mM) and 2-desoxyglucose (2-DG; 1 mM) for 2 min. Each image was collected for a period of 80 s. The first image was taken in ASCF ("T80"), before exposing the cells to the metabolic inhibitors (red bars) and generating three more images ("T160, T240, T320"). Bottom: [Na⁺] at each time point (mean ± SEM; *n* = 24) in the three compartments. Dotted line represents baseline [Na⁺] in the respective compartment. **(B)** Same experimental setup and illustration as in A, showing the effect of perfusion with nominally K⁺-free saline for 1 min (indicated by green bar; *n* = 17). **(A and B)** Scale bars, 20 µm. *, P < 0.05, **, P < 0.01, and ***, P ≤ 0.001.

by 4 s of time needed for saving the image), which is 10 times faster than required for TCSPC-based FLIM with pixel fluorescence decay analysis by fitting a sum of exponential decay functions. As observed before, all three cellular compartments exhibited a significant rise in [Na⁺] upon perfusion with K⁺-free saline (Fig. 5 C). After ∼3 min, [Na⁺] had increased by ∼15 mM. This increase was similar in amplitude to the values obtained using conventional FLIM at this time point (see Fig. 4 B). [Na⁺] continued to rise in all compartments for five to seven more minutes to a new plateau, 30–40 mM over the initial baseline. Again, no recovery was observed, suggesting a long-lasting inhibition of the NKA in response to removal of extracellular K⁺.

To determine the temporal onset of the [Na⁺] increase, the SD of the FL obtained under baseline conditions was calculated and the first time point at which the FL exceeded 2 × SD identified. This analysis revealed an increase in [Na⁺] about ∼72 s (71.9 ± 28.6 s) after K⁺ removal within the cytosolic compartment. Nucleus and perinuclear regions showed delayed responses of ∼92 s (92.3 ± 31.7 s) and ∼118 s (117.6 ± 42.1 s), respectively. Ratio FLIM thus uncovered a clear temporal sequence in the responses

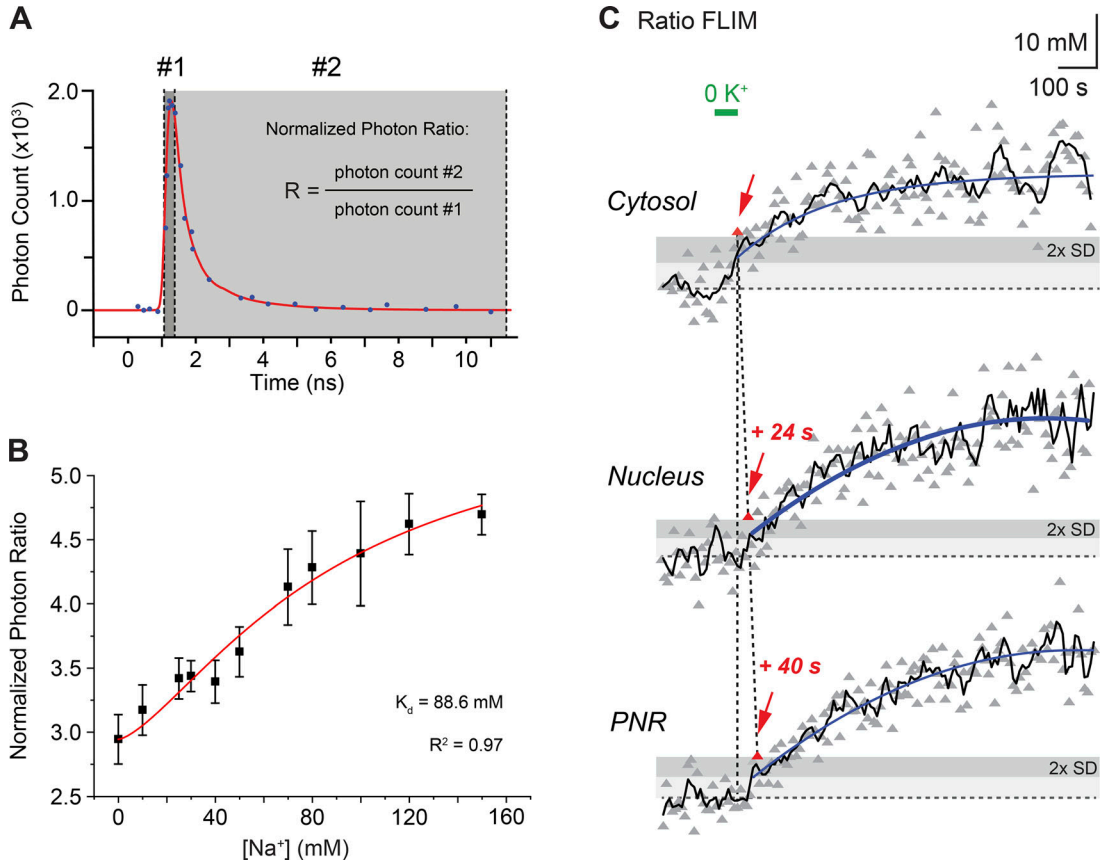

Figure 5. **"Ratio FLIM" of CoroNaGreen. (A)** Schematic illustration of the Ratio FLIM approach and the empirical separation of the photon distribution of the FL into two boxes (#1 from 1.12 to 1.37 ns and #2 from 1.37 to 11.52 ns), representing a fast and slow segment, respectively. The normalized photon ratio "R" is then expressed as the quotient of the photon counts of both segments as indicated. **(B)** Plot of the normalized photon ratio against the $[Na^+]$ (means ± SD; n = 18). Red line represents a sigmoidal fit (K_d =88.6; R^2 = 0.97). **(C)** Ratio FLIM of CoroNaGreen in a HEK cell, revealing changes in $[Na^+]$ in response to removal of extracellular K^+ (green bar) for 1 min in the three compartments. Gray triangles show individual data points; the black line represents a smoothened trace (Savitzky-Golay Filter 5); the dotted line indicates the average baseline value. The red arrows point to the first data point (colored in red) that exceeds 2× the SD (as depicted by the gray areas) in each compartment. Note the latency in the response of the nucleus (24 s) and PNR (40 s) as compared with the cytosol.

of the different subcellular compartments, with the cytosol leading the $[Na^+]$ increase, while the $[Na^+]$ increase occurred with a delay of another 20 s in the nucleus and 46 s in the perinuclear region as compared with the cytosol (Fig. 5 C).

In summary, these experiments show that ratiometric analysis of the FL of CoroNaGreen is suitable for the quantitative detection of $[Na^+]$ changes in subcellular compartments. As compared with conventional FLIM, the temporal resolution increases significantly by reducing the time required for image generation from 80 to 8 s.

Discussion

Suitability of CoroNaGreen FL for quantitative determination of $[Na^+]$ in situ

Our calibration of CoroNaGreen showed that it exhibits distinct changes in FL when binding Na^+ in the range between 0 and 150 mM both in vitro and in situ. As reported before (Rungta et al., 2015), the normalized decay curves were best fit with a bi-exponential function. In contrast to the former work, the average lifetime τ_{AVG} instead of τ_1 was used, as it proved a more stable fit parameter at our experimental setup. In HEK cells, when τ_{AVG} (obtained from ROIs positioned over nuclear and cytosolic regions) was plotted against $[Na^+]$, the data followed a sigmoidal curve revealing an apparent K_d of 79.9 mM. Earlier calibrations of CoroNaGreen's sensitivity for Na^+ performed in hippocampal neurons only covered the lower concentration range, still suggesting that CoroNaGreen's K_d for Na^+ is >60 mM (Meier et al., 2006). The data provided by Rungta et al. (2015), performing lifetime measurements with CoroNaGreen in hippocampal neurons, is also in line with this observation. Notably, the apparent K_d was significantly lower under in vitro conditions as compared with the calibrations performed in HEK cells, a phenomenon already observed for different other dyes including the sodium indicators Sodium Green (Szmacinski and Lakowicz, 1997; Despa et al., 2000b) and AsanteNatriumGreen 2 (Lamy and Chatton, 2011; Roder and Hille, 2014; Naumann et al., 2018).

CoroNaGreen's average FL (τ_{AVG}) in HEK cells increased from ~480 ps at 0 mM Na^+ to ~1,030 ps at 150 mM. This change in lifetime with binding of Na^+ is rather moderate as compared to, e.g., the calcium indicators OGB-1 and OGB-2 (Oregon-Green-BAPTA-1/2),

which undergo a more than fivefold increase in their FL upon binding of calcium (Wilms and Eilers, 2007; Zheng et al., 2018). Other commercially available Na^+ sensors tested so far either are not suited for FL imaging or only show moderate changes in lifetime as well.

The UV-excitable, ratiometric Na^+ indicator sodium-binding benzofuran isophthalate (Minta and Tsien, 1989) has been widely used for intensity-based quantitative imaging with wide-field microscopy (Schreiner and Rose, 2012) as well as with two-photon microscopy (Rose et al., 1999), but cannot be employed for FL imaging (Despa et al., 2000a; Naumann et al., 2018). Sodium Green, which exhibits an absorption maximum at 507 nm, was characterized using the frequency domain (Szmacinski and Lakowicz, 1997; Despa et al., 2000b), as well as time-correlated lifetime measurements (Biskup and Gensch, 2014; Naumann et al., 2018), the former revealing an increase in the lifetime of about twofold with binding of Na^+. Sodium Green, however, is difficult to reliably employ in situ, since it interacts strongly with cytosolic constituents leading to similar FL changes as caused by Na^+ binding (Biskup and Gensch, 2014). Finally, AsanteNatriumGreen 2 (now distributed by abcam as "ION NaTRIUM Green"), shows the most prominent changes in FL upon Na^+ binding compared with the aforementioned Na^+ indicators, but exhibits a notable sensitivity to K^+ as well as protons (pH; Roder and Hille, 2014; Naumann et al., 2018).

As mentioned above, CoroNaGreen has been employed for Na^+ lifetime imaging in situ before (Rungta et al., 2015). Because in the former work, the dyes' cross-selectivity to other ions was not tested, we also analyzed the K^+- and pH-sensitivity of CoroNaGreen in the present study. With $[Na^+]$ kept constant, our data demonstrate no sensitivity of CoroNaGreen FL to a reduction of K^+ from 120 to 80 mM, which is within a concentration range expected to occur during the manipulations performed in the present study (removal of extracellular K^+ and metabolic inhibition). Moreover, no dependence on pH at values between pH 6.0 and 8.0 was detected, while FL slightly increased at pH ≤5.5. We also found that CoroNaGreen's lifetime was independent from the presence of dextran up to a concentration of 5% (corresponding to a viscosity of roughly 2.5 mPa s; (Carrasco et al., 1989). Altogether, we thus conclude CoroNaGreen is generally suited for FL imaging of Na^+ inside cells.

Notably, possible differences in ionic concentrations or viscosity between different cellular subcompartments are not expected to strongly influence the FL properties of the dye. This is especially relevant considering the deviation of FL in perinuclear regions as compared with the nucleus and cytosol at $[Na^+]$ ≤50 mM (see Fig. 3 B). The perinuclear regions exhibiting a high FL/intensity strongly colocalized with Mitotracker fluorescence, indicating that they contain a high number of mitochondria. Moreover, perinuclear regions also host lysosomes, which have a pH of ∼5. The distinct difference in FL found in the perinuclear could thus at least be partly be due to a different behavior of the dye inside these two organelles (e.g., because of a different ionic or protein environment). The overlapping of the FL response of the three compartments at $[Na^+]$ >70 mM, however, argues against this notion.

Baseline $[Na^+]$ in cellular subcompartments

Our calibrations indicated that under baseline conditions (in physiological ACSF), mean $[Na^+]$ in the cytosol was at 17.6 mM, which is in the range of $[Na^+]_i$ determined in other cell types, including HeLa cells (12–14 mM; Despa et al., 2000b), vertebrate neurons (15 mM; Kelly and Rose, 2010) or astrocytes (17 mM; Unichenko et al., 2012). Nuclear regions exhibited a significantly smaller $[Na^+]$ (∼13 mM) than the cytosol. Earlier work using intensity-based imaging with Na^+ indicator dyes in different cell types concluded that cytosolic and nuclear $[Na^+]$ are similar (e.g., smooth muscle cells; Borin et al., 1993), and that nuclear $[Na^+]$ is lower than cytosolic $[Na^+]$ (e.g., ventricular myocytes [Kondratev and Gallitelli, 2003] and hepatocytes [Garner, 2002]), or the other way around (e.g., heart myocytes; Bkaily et al., 1997). Notably, while the nuclear pore complexes were long thought to represent the only pathway for ions, recent work has provided strong evidence for the presence of ion channels, transporters, and receptors in the nuclear membrane. These include the sodium/calcium exchanger (Secondo et al., 2018), sodium/proton exchanger (Bkaily et al., 2012), and NKA (Garner, 2002), all of which might be involved in setting nuclear $[Na^+]$. Still, while our data imply that the mean $[Na^+]$ in the nucleus is significantly lower than that of the cytosol, the biological relevance of this difference in $[Na^+]$ remains unclear at present.

In ACSF, the perinuclear areas of the cells exhibited an increased average FL as compared with the nucleus-far cytosolic areas and the nucleus itself, suggesting that $[Na^+]$ might differ between these compartments. Notably, our data suggest that the calibration procedure using ionophores that are preferentially inserted into the plasma membrane did not enable a reliable permeabilization of perinuclear organelles for $[Na^+]$ in the concentration range relevant for this study (0–50 mM). Therefore, we did not construct a separate calibration curve from this compartment. While different cellular compartments and organelles certainly differ in their chemical, ionic, and/or protein environment, our data also show that CoroNaGreen FL is rather insensitive to differences in K^+, pH, or viscosity. As argued above, we conclude from these results that the observed differences in FL were not related to a different behavior of the dye in the different compartments.

Our data suggest differences in the $[Na^+]$ between subcellular compartments, with perinuclear regions exhibiting an average $[Na^+]$ of ∼27 mM, a level significantly higher than the $[Na^+]$ of cytosolic as well as of nuclear regions. The perinuclear region is characterized by the presence of lysosomes and contains a high density of mitochondria as demonstrated by our Mitotracker stainings. Regions of high FL/intensity showed a remarkable overlap with Mitotracker fluorescence, suggesting that the high $[Na^+]$ in this region mainly reflects the $[Na^+]$ of mitochondria. In addition, it may, at least partly, report $[Na^+]$ of other organelles present, including endoplasmatic reticulum or lysosomes.

A difference between cytosolic and mitochondrial $[Na^+]$ was also found in an earlier study (Bernardinelli et al., 2006) using intensity-based fluorescence imaging with the red-shifted variant CoroNaRed, which preferentially enters mitochondria (see also Ben-Kasus Nissim et al., 2017).

Combining this with sodium-binding benzofuran isophthalate to monitor cytosolic [Na^+], they reported an elevated mitochondrial [Na^+] as compared with the cytosol (19 mM versus 13 mM; Bernardinelli et al., 2006). In contrast to this, other work indicated that mitochondrial [Na^+] might be several millimoles lower than cytosolic [Na^+] (e.g., Donoso et al., 1992; Murphy and Eisner, 2009). Na^+ uptake into mitochondria is mediated by the mitochondrial Na^+/Ca^{2+} exchanger (Palty et al., 2010; Nita et al., 2014; Ben-Kasus Nissim et al., 2017), which is antagonized by sodium efflux through a Na^+/H^+ exchanger (Bernardinelli et al., 2006; Nita et al., 2015). Na^+/Ca^{2+} exchanger activity is modulated by the cytoplasmic [Na^+] (Maack et al., 2006; Kim and Matsuoka, 2008), and depending on the driving forces, this transporter can switch between forward (Na^+ influx) and reverse (Na^+ efflux) mode (Samanta et al., 2018). Mitochondrial [Na^+] is thus likely to be set in a dynamic equilibrium, determined by ion concentrations and dynamics (Na^+, Ca^{2+}, pH) and the relative strength of Na^+ influx versus Na^+ efflux.

Detection of changes in [Na^+] using FLIM

To evaluate if FLIM of CoroNaGreen can be employed to reveal changes in [Na^+], we performed two experimental approaches expected to result in an increase in cellular [Na^+]. Metabolic inhibition by addition of blockers of glycolysis and mitochondrial respiration indeed caused significant changes in the FLs of CoroNaGreen in all three cellular compartments, indicative of an increase in their [Na^+] by 6–7 mM. Earlier work performed, e.g., in brain tissue, has shown that this induces a decrease in cellular ATP (Lerchundi et al., 2018), resulting in an inhibition of the NKA and an increase in cellular $[Na^+]_i$ (Gerkau et al., 2018).

Similarly, removal of extracellular K^+ for a period of 1 min resulted in increased FL in HEK cells, with an increase in [Na^+] by 13–16 mM as detected after 3 min in the cytosol, nucleus, and perinuclear region. The [Na^+] increase induced by removal of extracellular K^+ was thus larger than upon addition of metabolic blockers, most likely because the former induces an immediate and complete inhibition of the NKA. As a consequence, removal of K^+ causes a strong increase in the cellular $[Na^+]_i$ of many cell types, including neurons and astrocytes (e.g., Rose and Ransom, 1996b; Kelly and Rose, 2010).

Conventional FLIM inherits a rather low temporal resolution, and photons have to be collected over a period of 80 s for reliable fits of the pixel fluorescence decays. To increase the temporal resolution of our measurements, we introduced a modified data analysis, termed "ratiometric" photon counting (Minge et al., 2017; Zheng et al., 2018). With this approach, the photon distribution is empirically separated into a "fast" and a "slow" segment, and the quotient of both (the photon count ratio) is calculated. This procedure resulted in a strong reduction in photon collection periods and a 10-fold increase in temporal resolution to 0.125 Hz.

Ratio FLIM thereby enabled a better visualization of the dynamic onset and time course of the increase in [Na^+] induced by removal of K^+ in the three cellular compartments. Indeed, while it showed similar amplitudes as compared with conventional FLIM, it revealed a temporal sequence in the response time: cytosolic [Na^+] began to rise within ∼72 s upon the removal of potassium, whereas the rise in nuclear [Na^+] was delayed by an additional 20 s. The increase in the perinuclear area [Na^+] even lagged an additional 26 s behind. This sequence of events suggests that removal of extracellular K^+ first results in an inhibition of the plasma membrane NKA and in an increase in cytosolic [Na^+]. The disturbance of cytosolic [Na^+] then evokes a secondary increase in nuclear [Na^+] and, finally, in organelles present in the perinuclear region. Altogether, we conclude from these data that ratio FLIM is well suited to probe for dynamic changes in [Na^+] in different cellular compartments that occur within this time range.

Acknowledgments

Sharona E. Gordon served as editor.

We thank Simone Durry and Claudia Roderigo (Institute of Neurobiology, Heinrich Heine University, Düsseldorf, Germany) for excellent technical assistance, as well as Bettina Mertens, Andrea Jansen, and Hua Tan (Forschungszentrum Jülich, ICS-4, Germany) for excellent support with cell culture. We also thank Dr. Christian Henneberger (Bonn University) for helpful comments and advice on data analysis.

J. Meyer was supported by the International Helmholtz Research School of Biophysics and Soft Matter, Forschungszentrum Jülich, Germany. This work was supported by the Deutsche Forschungsgemeinschaft (Ro2327/8-2 and 13-1).

The authors declare no competing financial interests.

Author contributions: All authors had full access to all the data in the study and take responsibility for the integrity of the data and the accuracy of the data analysis. J. Meyer, V. Untiet, C. Fahlke, T. Gensch, C.R. Rose: design and conceptualization of research, data analysis; J. Meyer, V. Untiet, T. Gensch: experiments and data analysis; J. Meyer, T. Gensch, C.R. Rose: writing original draft; J. Meyer, V. Untiet, C. Fahlke, T. Gensch, C.R. Rose: review and editing of the manuscript; C. Fahlke, C.R. Rose: funding acquisition.

Submitted: 6 June 2019
Accepted: 11 September 2019

References

Aronsen, J.M., F. Swift, and O.M. Sejersted. 2013. Cardiac sodium transport and excitation-contraction coupling. *J. Mol. Cell. Cardiol.* 61:11–19. https://doi.org/10.1016/j.yjmcc.2013.06.003

Ballanyi, K., P. Grafe, and G. ten Bruggencate. 1983. Intracellular free sodium and potassium, post-carbachol hyperpolarization, and extracellular potassium-undershoot in rat sympathetic neurones. *Neurosci. Lett.* 38: 275–279. https://doi.org/10.1016/0304-3940(83)90381-6

Bastiaens, P.I., and A. Squire. 1999. Fluorescence lifetime imaging microscopy: spatial resolution of biochemical processes in the cell. *Trends Cell Biol.* 9:48–52. https://doi.org/10.1016/S0962-8924(98)01410-X

Becker, W. 2005. *Advanced Time-Correlated Single Photon Counting Techniques*. Springer-Verlag, Berlin Heidelberg.

Becker, W. 2012. Fluorescence lifetime imaging--techniques and applications. *J. Microsc.* 247:119–136. https://doi.org/10.1111/j.1365-2818.2012.03618.x

Ben-Kasus Nissim, T., X. Zhang, A. Elazar, S. Roy, J.A. Stolwijk, Y. Zhou, R.K. Motiani, M. Gueguinou, N. Hempel, M. Hershfinkel, et al. 2017. Mitochondria control store-operated Ca^{2+} entry through Na^+ and redox signals. *EMBO J.* 36:797–815. https://doi.org/10.15252/embj.201592481

Bernardinelli, Y., G. Azarias, and J.Y. Chatton. 2006. In situ fluorescence imaging of glutamate-evoked mitochondrial Na^+ responses in astrocytes. *Glia.* 54:460–470. https://doi.org/10.1002/glia.20387

Biskup, C., and T. Gensch. 2014. Fluorescence lifetime imaging of ions in biological tissues. In *Fluorescence Lifetime Spectroscopy and Imaging. Principles and Applications in Biomedical Diagnostics.* D. Elson, F.P.W.M. French, and L. Marcu, editors. Taylor & Francis, Boca Raton. 24.

Bkaily, G., D. Jaalouk, G. Haddad, N. Gros-Louis, M. Simaan, R. Naik, and P. Pothier. 1997. Modulation of cytosolic and nuclear Ca^{2+} and Na^+ transport by taurine in heart cells. *Mol. Cell. Biochem.* 170:1–8. https://doi.org/10.1023/A:1006879918371

Bkaily, G., L. Avedanian, J. Al-Khoury, L. Ahmarani, C. Perreault, and D. Jacques. 2012. Receptors and ionic transporters in nuclear membranes: new targets for therapeutical pharmacological interventions. *Can. J. Physiol. Pharmacol.* 90:953–965. https://doi.org/10.1139/y2012-077

Borin, M.L., W.F. Goldman, and M.P. Blaustein. 1993. Intracellular free Na^+ in resting and activated A7r5 vascular smooth muscle cells. *Am. J. Physiol.* 264:C1513–C1524. https://doi.org/10.1152/ajpcell.1993.264.6.C1513

Carrasco, F., E. Chornet, R.P. Overend, and J. Costa. 1989. A generalized correlation for the viscosity of dextrans in aqueous solutions as a function of temperature, concentration, and molecular weight at low shear rates. *J. Appl. Polym. Sci.* 37:2087–2098. https://doi.org/10.1002/app.1989.070370801

Despa, S., P. Steels, and M. Ameloot. 2000a. Fluorescence lifetime microscopy of the sodium indicator sodium-binding benzofuran isophthalate in HeLa cells. *Anal. Biochem.* 280:227–241. https://doi.org/10.1006/abio.2000.4505

Despa, S., J. Vecer, P. Steels, and M. Ameloot. 2000b. Fluorescence lifetime microscopy of the Na^+ indicator Sodium Green in HeLa cells. *Anal. Biochem.* 281:159–175. https://doi.org/10.1006/abio.2000.4560

Donoso, P., J.G. Mill, S.C. O'Neill, and D.A. Eisner. 1992. Fluorescence measurements of cytoplasmic and mitochondrial sodium concentration in rat ventricular myocytes. *J. Physiol.* 448:493–509. https://doi.org/10.1113/jphysiol.1992.sp019053

Garner, M.H. 2002. Na,K-ATPase in the nuclear envelope regulates Na^+: K^+ gradients in hepatocyte nuclei. *J. Membr. Biol.* 187:97–115. https://doi.org/10.1007/s00232-001-0155-5

Gerkau, N.J., C. Rakers, S. Durry, G.C. Petzold, and C.R. Rose. 2018. Reverse NCX attenuates cellular sodium loading in metabolically compromised cortex. *Cereb. Cortex.* 28:4264–4280. https://doi.org/10.1093/cercor/bhx280

Gilbert, D., C. Franjic-Würtz, K. Funk, T. Gensch, S. Frings, and F. Möhrlen. 2007. Differential maturation of chloride homeostasis in primary afferent neurons of the somatosensory system. *Int. J. Dev. Neurosci.* 25:479–489. https://doi.org/10.1016/j.ijdevneu.2007.08.001

Harootunian, A.T., J.P. Kao, B.K. Eckert, and R.Y. Tsien. 1989. Fluorescence ratio imaging of cytosolic free Na^+ in individual fibroblasts and lymphocytes. *J. Biol. Chem.* 264:19458–19467.

Kaneko, H., I. Putzier, S. Frings, U.B. Kaupp, and T. Gensch. 2004. Chloride accumulation in mammalian olfactory sensory neurons. *J. Neurosci.* 24:7931–7938. https://doi.org/10.1523/JNEUROSCI.2115-04.2004

Kaplan, J.H. 2002. Biochemistry of Na,K-ATPase. *Annu. Rev. Biochem.* 71:511–535. https://doi.org/10.1146/annurev.biochem.71.102201.141218

Kelly, T., and C.R. Rose. 2010. Ammonium influx pathways into astrocytes and neurones of hippocampal slices. *J. Neurochem.* 115:1123–1136. https://doi.org/10.1111/j.1471-4159.2010.07009.x

Kim, B., and S. Matsuoka. 2008. Cytoplasmic Na^+-dependent modulation of mitochondrial Ca^{2+} via electrogenic mitochondrial Na^+-Ca^{2+} exchange. *J. Physiol.* 586:1683–1697. https://doi.org/10.1113/jphysiol.2007.148726

Kirischuk, S., V. Parpura, and A. Verkhratsky. 2012. Sodium dynamics: another key to astroglial excitability? *Trends Neurosci.* 35:497–506. https://doi.org/10.1016/j.tins.2012.04.003

Kofuji, P., and E.A. Newman. 2004. Potassium buffering in the central nervous system. *Neuroscience.* 129:1045–1056. https://doi.org/10.1016/j.neuroscience.2004.06.008

Kondratev, D., and M.F. Gallitelli. 2003. Increments in the concentrations of sodium and calcium in cell compartments of stretched mouse ventricular myocytes. *Cell Calcium.* 34:193–203. https://doi.org/10.1016/S0143-4160(03)00084-8

Kuchibhotla, K.V., C.R. Lattarulo, B.T. Hyman, and B.J. Bacskai. 2009. Synchronous hyperactivity and intercellular calcium waves in astrocytes in Alzheimer mice. *Science.* 323:1211–1215. https://doi.org/10.1126/science.1169096

Lahn, M., C. Dosche, and C. Hille. 2011. Two-photon microscopy and fluorescence lifetime imaging reveal stimulus-induced intracellular Na^+ and Cl^- changes in cockroach salivary acinar cells. *Am. J. Physiol. Cell Physiol.* 300:C1323–C1336. https://doi.org/10.1152/ajpcell.00320.2010

Lakowicz, J.R., H. Szmacinski, K. Nowaczyk, and M.L. Johnson. 1992. Fluorescence lifetime imaging of calcium using Quin-2. *Cell Calcium.* 13:131–147. https://doi.org/10.1016/0143-4160(92)90041-P

Lamy, C.M., and J.Y. Chatton. 2011. Optical probing of sodium dynamics in neurons and astrocytes. *Neuroimage.* 58:572–578. https://doi.org/10.1016/j.neuroimage.2011.06.074

Langer, J., and C.R. Rose. 2009. Synaptically induced sodium signals in hippocampal astrocytes in situ. *J. Physiol.* 587:5859–5877. https://doi.org/10.1113/jphysiol.2009.182279

Lerchundi, R., K.W. Kafitz, U. Winkler, M. Farfers, J. Hirrlinger, and C.R. Rose. 2018. FRET-based imaging of intracellular ATP in organotypic brain slices. *J. Neurosci. Res.* 1:•••; (Epub ahead of print). https://doi.org/10.1002/jnr.24361

Maack, C., S. Cortassa, M.A. Aon, A.N. Ganesan, T. Liu, and B. O'Rourke. 2006. Elevated cytosolic Na^+ decreases mitochondrial Ca^{2+} uptake during excitation-contraction coupling and impairs energetic adaptation in cardiac myocytes. *Circ. Res.* 99:172–182. https://doi.org/10.1161/01.RES.0000232546.92777.05

Meier, S.D., Y. Kovalchuk, and C.R. Rose. 2006. Properties of the new fluorescent Na^+ indicator CoroNa Green: comparison with SBFI and confocal Na^+ imaging. *J. Neurosci. Methods.* 155:251–259. https://doi.org/10.1016/j.jneumeth.2006.01.009

Minge, D., O. Senkov, R. Kaushik, M.K. Herde, O. Tikhobrazova, A.B. Wulff, A. Mironov, T.H. van Kuppevelt, A. Oosterhof, G. Kochlamazashvili, et al. 2017. Heparan Sulfates Support Pyramidal Cell Excitability, Synaptic Plasticity, and Context Discrimination. *Cereb. Cortex.* 27:903–918.

Minta, A., and R.Y. Tsien. 1989. Fluorescent indicators for cytosolic sodium. *J. Biol. Chem.* 264:19449–19457.

Murphy, E., and D.A. Eisner. 2009. Regulation of intracellular and mitochondrial sodium in health and disease. *Circ. Res.* 104:292–303. https://doi.org/10.1161/CIRCRESAHA.108.189050

Naumann, G., K. Lippmann, and J. Eilers. 2018. Photophysical properties of Na^+-indicator dyes suitable for quantitative two-photon fluorescence-lifetime measurements. *J. Microsc.* 272:136–144. https://doi.org/10.1111/jmi.12754

Nita, I.I., M. Hershfinkel, C. Kantor, G.A. Rutter, E.C. Lewis, and I. Sekler. 2014. Pancreatic β-cell Na+ channels control global Ca2+ signaling and oxidative metabolism by inducing Na+ and Ca2+ responses that are propagated into mitochondria. *FASEB J.* 28:3301–3312. https://doi.org/10.1096/fj.13-248161

Nita, I.I., M. Hershfinkel, E.C. Lewis, and I. Sekler. 2015. A crosstalk between Na^+ channels, Na^+/K^+ pump and mitochondrial Na^+ transporters controls glucose-dependent cytosolic and mitochondrial Na^+ signals. *Cell Calcium.* 57:69–75. https://doi.org/10.1016/j.ceca.2014.12.007

Palty, R., W.F. Silverman, M. Hershfinkel, T. Caporale, S.L. Sensi, J. Parnis, C. Nolte, D. Fishman, V. Shoshan-Barmatz, S. Herrmann, et al. 2010. NCLX is an essential component of mitochondrial Na^+/Ca^{2+} exchange. *Proc. Natl. Acad. Sci. USA.* 107:436–441. https://doi.org/10.1073/pnas.0908099107

Parnis, J., V. Montana, I. Delgado-Martinez, V. Matyash, V. Parpura, H. Kettenmann, I. Sekler, and C. Nolte. 2013. Mitochondrial exchanger NCLX plays a major role in the intracellular Ca^{2+} signaling, gliotransmission, and proliferation of astrocytes. *J. Neurosci.* 33:7206–7219. https://doi.org/10.1523/JNEUROSCI.5721-12.2013

Roder, P., and C. Hille. 2014. ANG-2 for quantitative Na(+) determination in living cells by time-resolved fluorescence microscopy. *Photochem. Photobiol. Sci.* 13:1699–1710. https://doi.org/10.1039/C4PP00061G

Rose, C.R., and B.R. Ransom. 1996a. Intracellular sodium homeostasis in rat hippocampal astrocytes. *J. Physiol.* 491:291–305. https://doi.org/10.1113/jphysiol.1996.sp021216

Rose, C.R., and B.R. Ransom. 1996b. Mechanisms of H^+ and Na^+ changes induced by glutamate, kainate, and D-aspartate in rat hippocampal astrocytes. *J. Neurosci.* 16:5393–5404. https://doi.org/10.1523/JNEUROSCI.16-17-05393.1996

Rose, C.R., Y. Kovalchuk, J. Eilers, and A. Konnerth. 1999. Two-photon Na^+ imaging in spines and fine dendrites of central neurons. *Pflugers Arch.* 439:201–207.

Rungta, R.L., H.B. Choi, J.R. Tyson, A. Malik, L. Dissing-Olesen, P.J.C. Lin, S.M. Cain, P.R. Cullis, T.P. Snutch, and B.A. MacVicar. 2015. The cellular mechanisms of neuronal swelling underlying cytotoxic edema. *Cell.* 161:610–621. https://doi.org/10.1016/j.cell.2015.03.029

Samanta, K., G.R. Mirams, and A.B. Parekh. 2018. Sequential forward and reverse transport of the Na^+ Ca^{2+} exchanger generates Ca^{2+} oscillations within mitochondria. *Nat. Commun.* 9:156. https://doi.org/10.1038/s41467-017-02638-2

Schneider, C.A., W.S. Rasband, and K.W. Eliceiri. 2012. NIH Image to ImageJ: 25 years of image analysis. *Nat. Methods.* 9:671–675. https://doi.org/10.1038/nmeth.2089

Schreiner, A.E., and C.R. Rose. 2012. Quantitative Imaging of Intracellular Sodium. In *Current microscopy contributions to advances in science and technology*. A. Méndez-Vilas, editor. Formatex Research Center, Badajoz, Spain. 119–129. Microscopy Book Series.

Secondo, A., A. Esposito, T. Petrozziello, F. Boscia, P. Molinaro, V. Tedeschi, A. Pannaccione, R. Ciccone, N. Guida, G. Di Renzo, and L. Annunziato. 2018. Na^+/Ca^{2+} exchanger 1 on nuclear envelope controls PTEN/Akt pathway via nucleoplasmic Ca^{2+} regulation during neuronal differentiation. *Cell Death Discov.* 4:12. https://doi.org/10.1038/s41420-017-0018-1

Suhling, K., P.M. French, and D. Phillips. 2005. Time-resolved fluorescence microscopy. *Photochem. Photobiol. Sci.* 4:13–22.

Sweadner, K.J. 1989. Isozymes of the Na^+/K^+-ATPase. *Biochim. Biophys. Acta.* 988:185–220. https://doi.org/10.1016/0304-4157(89)90019-1

Szmacinski, H., and J.R. Lakowicz. 1997. Sodium Green as a potential probe for intracellular sodium imaging based on fluorescence lifetime. *Anal. Biochem.* 250:131–138. https://doi.org/10.1006/abio.1997.2203

Unichenko, P., O. Myakhar, and S. Kirischuk. 2012. Intracellular Na+ concentration influences short-term plasticity of glutamate transporter-mediated currents in neocortical astrocytes. *Glia.* 60:605–614. https://doi.org/10.1002/glia.22294

Untiet, V., L.M. Moeller, X. Ibarra-Soria, G. Sánchez-Andrade, M. Stricker, E.M. Neuhaus, D.W. Logan, T. Gensch, and M. Spehr. 2016. Elevated Cytosolic Cl- Concentrations in Dendritic Knobs of Mouse Vomeronasal Sensory Neurons. *Chem. Senses.* 41:669–676. https://doi.org/10.1093/chemse/bjw077

Untiet, V., P. Kovermann, N.J. Gerkau, T. Gensch, C.R. Rose, and C. Fahlke. 2017. Glutamate transporter-associated anion channels adjust intracellular chloride concentrations during glial maturation. *Glia.* 65:388–400. https://doi.org/10.1002/glia.23098

Verkhratsky, A., M. Trebak, F. Perocchi, D. Khananshvili, and I. Sekler. 2018. Crosslink between calcium and sodium signalling. *Exp. Physiol.* 103:157–169. https://doi.org/10.1113/EP086534

Wilms, C.D., and J. Eilers. 2007. Photo-physical properties of Ca^{2+}-indicator dyes suitable for two-photon fluorescence-lifetime recordings. *J. Microsc.* 225:209–213. https://doi.org/10.1111/j.1365-2818.2007.01746.x

Wilms, C.D., H. Schmidt, and J. Eilers. 2006. Quantitative two-photon Ca^{2+} imaging via fluorescence lifetime analysis. *Cell Calcium.* 40:73–79. https://doi.org/10.1016/j.ceca.2006.03.006

Wright, E.M., and E. Turk. 2004. The sodium/glucose cotransport family SLC5. *Pflugers Arch.* 447:510–518. https://doi.org/10.1007/s00424-003-1202-0

Zheng, K., L. Bard, J.P. Reynolds, C. King, T.P. Jensen, A.V. Gourine, and D.A. Rusakov. 2015. Time-Resolved Imaging Reveals Heterogeneous Landscapes of Nanomolar Ca(2+) in Neurons and Astroglia. *Neuron.* 88:277–288. https://doi.org/10.1016/j.neuron.2015.09.043

Zheng, K., T.P. Jensen, and D.A. Rusakov. 2018. Monitoring intracellular nanomolar calcium using fluorescence lifetime imaging. *Nat. Protoc.* 13:581–597. https://doi.org/10.1038/nprot.2017.154